ACS APPLIED MATERIALS & INTERFACES

RESEARCH ARTICLE

www.acsami.org

A New Approach toward Carbon-Modified Vanadium-Doped Titanium Dioxide Photocatalysts

Haibei Liu, Yongmei Wu, and Jinlong Zhang*

Key Lab for Advanced Materials and Institute of Fine Chemicals, East China University of Science and Technology, 130 Meilong Road, Shanghai, 200237, P. R. China

Supporting Information

ABSTRACT: Carbon-modified vanadium-doped TiO_2 was successfully prepared with the intention of enhancing the visible-light photocatalytic performance by expanding the absorption in the visible-light region and improving the quantum efficiency of the photocatalytic reaction. The physicochemical properties of the catalysts were characterized by XRD, Raman, TEM, XPS, UV−vis diffuse reflectance spectra. The result indicated that some vanadium ions substituted for Ti^{4+} in the lattice of TiO_2, whereas all the carbon was modified on the surface of catalysts in the form of stable graphite-like carbonaceous species. Compared with vanadium doped TiO_2 sample and carbon modified TiO_2 sample, the 0.32C−0.5%V−TiO_2 photocatalyst exhibited excellent visible light activity and the synergistic effects of vanadium and carbon was responsible for improving the photocatalytic activity.

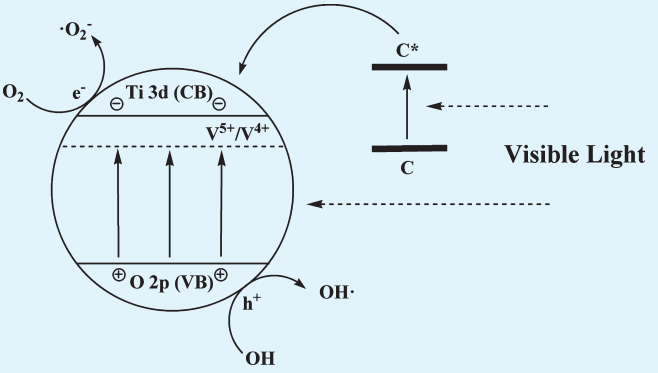

KEYWORDS: TiO_2, carbon modified, vanadium doped, photocatalytic activity

1. INTRODUCTION

Since Fujishima and Honda discovery the photoelectrochemical splitting of water on n-TiO_2 electrodes,[1] TiO_2 is of great interest in many current and emerging areas, for example, solar energy conversion, water spitting, and environmental applications.[2−4] Because of its high photoactivity, high chemical stability, low cost, and nontoxicity, lots of investigation have been carried on.

However, the band energy gap of TiO_2 is about 3.2 eV in the anatase crystalline phase, which is too wide to absorb visible light. Therefore, developing a novel method that provides TiO_2 photocatalyst with sufficient photosensitivity in the visible light region has been the major research effort in the recent years. For this purpose, many methods have been investigated; including nonmetal, transition metal and rare earth element doping, noble metal deposition, semiconductor coupled and dye sensitization,[5−11] etc. Among them, the transition-metal-doped TiO_2 is highly visible-active relatively, and lots of works on it have been reported.[12−23] Among these dopants, vanadium has been found to be the most effective in enhancing TiO_2 photocatalytic activity,[24−28] which corresponds to the enhanced absorption in the visible light region and reduction of particle size into nanometer range with high surface area and the improved quantum efficiency leading to improvement of the e^-−h^+ pair separation efficiency.

Moreover, another approach to synthesize visible-light photocatalysts is the nonmetal doping or modification. Carbon was reported to be effective in improving the activity of TiO_2 photocatalyst.[29,30] Carbon doping can produce a new hybrid state in the band gap, which narrows the band gap and therefore leads to significant visible light absorbance of the doped TiO_2. Furthermore, the carbon coated on TiO_2 particles could enhance adsorption of dyes (organic compounds) on the surface of the photocatalysts. Therefore, a great number of works has focused on carbon modification recently.[31−33] In our group, carbon-modified TiO_2 and carbon-co-modified TiO_2 with other metal or nonmetal have been studied for years.[34−37]

To the best of our knowledge, few studies address vanadium and carbon codoped/modified TiO_2. Some researchers use organic titanium precursor such as titanium isopropoxide (TTIP) or titanium tetrabutoxide (TBOT), which also has carbon in the precursor.[27] Therefore, it is hard to find out where the carbon comes from and difficult to calculate the real amount existed in the photocatalyst. And some researchers load V_2O_5 on the surface of carbon-doped TiO_2 to constitute a compound semiconductor,[24] which should be considered as another approach to improve photocatalytic activity.

In this study, the carbon-modified vanadium-doped TiO_2 catalyst was synthesized by a novel method using inorganic titanium tetrachloride as titanium precursor, ammonium metavanadate as vanadium precursor and glucose as carbon precursor. The resulting composite photocatalysts were systematically investigated by various techniques. And based on the characterization

Received: February 28, 2011
Accepted: April 19, 2011
Published: April 19, 2011

results, the effect of V and C on the photocatalytic performance of TiO_2 was discussed.

2. EXPERIMENTAL SECTION

2.1. Preparation of Photocatalysts. Low-temperature wet chemical method was used to obtain the carbon-modified vanadium-doped TO_2 photocatalysts. $TiCl_4$, NH_4VO_3, and glucose were used as the precursors of Ti, V, and C, respectively, and all chemicals used were of analytical reagent grade without further purification. First, 4.0 mL of $TiCl_4$ was added dropwise to 100 mL of iced distilled water under vigorous stirring, which was continuously stirred for 24 h. Afterward, ammonia aqueous solution was added to adjust the pH value to 7 to completely get $Ti(OH)_4$ precipitation, which was then filtered and washed by distilled water several times. The clean $Ti(OH)_4$ precipitation was dispersed again in distilled water (4 °C), and 30% H_2O_2 was added until it became a yellow solution accompanied by vigorous stirring. Then, different amounts of NH_4VO_3 were added in the transparent solution. The transparent solutions were following heated at 100 °C in a flask at air pressure for 48 h to get the crystalline hydrosol. The hydrosol was dried in vacuum at 60 °C for 10 h to get the powder, which was then calcined at 300 °C for 2 h to get the catalyst. A series of V-doped TiO_2 hydrosols were prepared by changing the V/Ti ratio. The obtained photocatalysts were denoted as x%V-TiO_2, where x% was the mole ratio of doped vanadium to titanium dioxide, which was varied from 0.3 to 1.0%. In addition, an undoped TiO_2 sample, which was denoted as blank-TiO_2, was prepared by the same procedure in the absence of NH_4VO_3 for comparison.

The carbon-modified samples were synthesized by hydrothermal treatment of the suspension of uncalcined V-doped TiO_2 with different amount of glucose at different molar ratios of C:Ti. And then the powders were calcined at 300 °C for 2 h to get the final catalyst. The obtained photocatalysts were denoted as $y-x$%V-TiO_2, where y was the mole ratio of modified carbon to titanium dioxide, which was varied from 0.16 to 0.48. A blank sample was also synthesized by hydrothermal treatment of blank-TiO_2 with distilled water only for comparison.

2.2. Characterization of Photocatalysts. XRD analysis of the prepared photocatalysts was carried out at room temperature with a Rigaku D/max 2550 VB/PC apparatus using Cu Kα radiation (λ = 0.5406 Å) and a graphite monchromator, operated at 40 kV and 30 mA. Diffraction patterns were recorded in the angular range of 10−80° with a stepwidth of 0.02° s^{-1}. UV−vis absorption spectra were obtained using a scan UV−vis spectrophotometer (Varian Cary 500) equipped with an integrating sphere assembly, while $BaSO_4$ was used as a reference. Raman measurements were performed at room temperature using an inVia Reflex Raman spectrometer with the excitation light of 514 nm. The surface morphologies and particle sizes were observed by high-resolution transmission electron microscopy (HRTEM, JEM-2011), using an accelerating voltage of 200 kV. Thermo gravimetric and differential thermal analysis (TG-DTA) curves were recorded on a Rigaku TG8120 instrument at a heating rate of 10 °C min^{-1} under air using R-Al_2O_3 as the standard material. To investigate the chemical states of the photocatalysts, werecorded X-ray photoelectron spectroscopy (XPS) with a Perkin-Elmer PHI 5000C ESCA System with Al Kα radiation operated at 250 W. The shift of binding energy due to relative surface charging was corrected using the C 1s level at 284.6 eV as an internal standard.

2.3. Photocatalytic Activity Test. The photocatalytic activity of each photocatalyst was measured in terms of degradation of Acid Orange 7 (AO7). Because AO7 is a common contaminant in industrial wastewater and has good resistance to light degradation, hence was selected as a model pollutant. A 1000 W tungsten halogen lamp equipped with a UV cutoff filters (λ > 420 nm) was used as a visible light source (the average light intensity was 60 mW cm^{-2}). And the lamp has a quartz cylindrical jacket around the lamp, in which the running water was used to keep the ambient temperature cool during the photocatalytic reaction. In a typical photocatalytic reaction, 0.08 g of photocatalyst was added into a 100 mL quartz tube photoreactor containing 80 mL of 20 mg L^{-1} AO7 solution. So the concentration of the photocatalyst would be 1 g L^{-1}. The mixture was stirred for 30 min in the dark to reach the adsorption−desorption equilibrium, and then put into the pohtocatalytic equipment. At the given time intervals, the analytical samples were taken from the mixture and immediately centrifuged to remove the photocatalysts. The concentration of the filtrate was analyzed by checking the absorbance at 483 nm with a UV−vis spectrophotometer (Varian Cary 100).

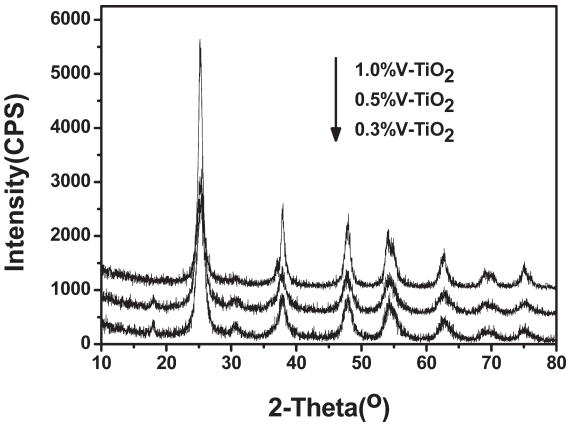

Figure 1. XRD patterns of 0.3%V-TiO_2, 0.5%V-TiO_2, and 1.0%V-TiO_2.

3. RESULTS AND DISCUSSION

3.1. X-ray Diffraction. Figure 1 shows the XRD patterns of different amount of V-doped TiO_2 nanoparticles, which indicates all of these samples, are mixed phases of anatase and brookite phases. No characteristic peaks of vanadium oxide (V_2O_5 and V_2O_4) are found, implying either V ions are incorporated in TiO_2 lattice or V oxides are very small and highly dispersed, which cannot be detected by XRD technique. And according to the phase formula reported before,[38] the percentage of the brookite of 0.3%V-TiO_2, 0.5%V-TiO_2, and 1%V-TiO_2 samples are 18.1, 17.8, and 10.9%, respectively, which decreases as the increasing of the dopant amount. Furthermore, the calculated average anatase crystallite sizes of these particles using Scherrer's formula are 7.7 nm, 8.3 and 10.9 nm, respectively, which indicates that doping V in TiO_2 lattice is beneficial to the growth of the TiO_2 nanoparticles. It is also noticed that for the (101) plane peak, a small shift occurs in the peak position after the introduction of V. And Table 1 shows the lattice parameters calculated by the XRD results. Compared with these of pure TiO_2, It is clear that the lattice parameters remain almost unchanged along the a-axis, whereas the c-axis parameters decrease as vanadium doped. Because the ionic radii of V^{4+} and V^{5+} are 0.58 and 0.54 Å, respectively, whereas Ti^{4+} ionic radius is 0.61 Å,[39] it can be concluded that the crystal lattice distortion is caused by the substitution of part of the Ti site by vanadium ions.

As is well-known, anatase is tetragonal while brookite is orthorhombic, and the theoretical density of brookite is greater than that of anatase, which means brookite is more compact and ordered than anatase. Therefore, it is easier to form anatase rather than brookite while vanadium ions replace Ti ions. Moreover, because the stacks of TiO_6 octahedra along the **a** (100) and **b** (010) directions in bulk brookite have patterns close to those in

Table 1. XRD Results of Different Amounts of Vanadium-Doped Samples

samples	crystal size of anatase (nm)	lattice parameters (Å)[a] *a*-axis	lattice parameters (Å)[a] *c*-axis	percentage of brookite (%)
blank-TiO_2	6.9	3.7827	9.5120	20.1
0.3%V-TiO_2	7.7	3.7801	9.4922	18.1
0.5%V-TiO_2	8.3	3.7839	9.4887	17.8
1.0%V-TiO_2	10.9	3.7870	9.4856	10.9

[a] Derived on the basis of Bragg's Law, $2d_{hkl}\sin\theta = n\lambda$ (with d^{101}), and the formula for a tetragonal unit cell: $1/(d_{hkl})^2 = (h^2 + k^2)/a^2 + l^2/c^2$. Here, d_{hkl} is the lattice spacing, θ is the incident angle, n is an integer, λ denotes the wavelength of the incident wave, (a, c) are the lattice parameters, and (h, k, l) represent the Miller indices (the error limits of crystal size and percentage are 1%, the error limits of lattice parameters are 0.1%)

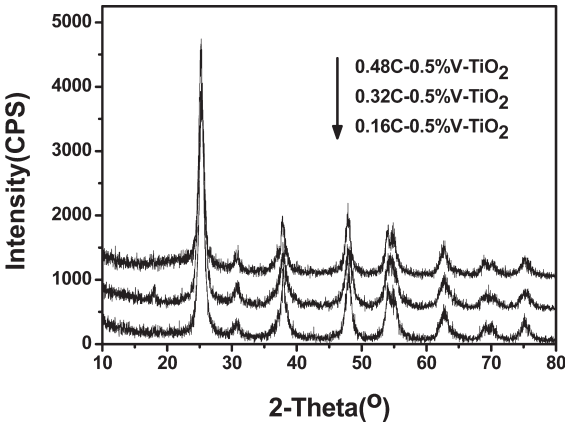

Figure 2. XRD patterns of 0.16C-0.5%V-TiO_2, 0.32C-0.5%V-TiO_2, and 0.48C-0.5%V-TiO_2.

anatase, corresponding anatase surfaces for those brookite surface planes cut through the *a* and/or *b* axes can be found, which are (112) and (110) surfaces.[40] So the formation of brookite from anatase by a solid state reaction is possible. However, the activation barrier for the transformation is the energy needed to displace octahedral cations into adjacent sites within a structure otherwise only slightly modified by distortion.[41] As concluded above, more vanadium doping can lead to more crystal lattice distortion, which is detrimental to the transformation brookite from anatase. Hence the more vanadium-doped, the less the percentage of brookite is.

And since TiO_6 octahedra grow in different directions in the lattice of anatase and brookite, the existence of brookite will suppress the growth of anatase near the interface. Therefore, the sample with higher percentage of brookite has smaller anatase crystallite size.[41] This result is a little bit different from the usual trend of doped TiO_2, whose particle size decrease as the increase of the dopant.[17,21] However, it should be noticed that, in their conditions, the catalysts are anatase only, whereas the samples prepared here are mixed phases of anatase and brookite.

Figure 2 exhibits the XRD patterns of different amount of carbon-modified 0.5% V-doped TiO_2 nanopaticles. It is evident that the brookite phase still exists after carbon modification, and the ratio of anatase to brookite rarely changes. Furthermore, as the carbon amount increases, the catalyst particle size increases slightly (10−12 nm), implying that carbon is well-coated on the surface of catalysts. These results indicate that the influence of carbon modification on the crystal structure is slight.

3.2. TEM Analysis. Figure 3 shows the TEM and HRTEM photos of 0.32C-0.5%V-TiO_2 with the SAED modes. It can be seen that the particle shape is short stick. The high-resolution TEM image reveals details of the crystallite size and crystalline phase. On the basis of the 0.35 nm *d*-spacing (region a), the nanostructure is in the anatase form (101) or brookite form (120) in the region studied, which is consistent with the powder XRD data. And there also exists 0.29 nm *d*-spacing (region b), which is assigned to the (121) planes of brookite. TEM images and corresponding XRD results indicate that the samples prepared have mixture of anatase and brookite phases.

No V−O compounds can be observed separately or on the TiO_2 particle surface, indicating that V ions have been incorporated into TiO_2 lattice, which accorded with the conclusion drawn from the SAED modes and Raman and XRD analysis.

3.3. UV−Vis Diffuse Reflectance Spectra. The UV−Vis diffuse reflectance spectra of samples prepared with different amount of vanadium are presented in Figure 4. The optical absorption edges of the V-TiO_2 are varied with the different percentage of vanadium doped. Vanadium doping into the atomic lattice of TiO_2 decreases the band gap and thus has a red shift in UV−Vis absorption band. And the absorption becomes broader with an increase in dopant amount.

The DRS of 0.5%V-TiO_2 samples modified with different amounts of carbon are illustrated in Figure 5. The more enhanced absorption observed in the visible region can be attributed to the presence of carbon on the surface. And the intensity of absorption shoulder between 400 and 800 nm increases with increasing carbon content. The sample with ratio of C:Ti = 0.48 shows the biggest absorption. This demonstrates that carbon modification can greatly enhance the photon absorption of V-TiO_2 in the region of visible light.

3.4. Raman Spectra. Figure 6 shows the Raman spectrum recorded under ambient conditions for blank sample, 0.5%V-TiO_2 and 0.32C-0.5%V -TiO_2. The Raman spectra of all the samples are characterized by a strong band at 142 cm^{-1}, three middle intensity bands at 395, 515, and 636 cm^{-1}. These peaks can be assigned to the fundamental vibration modes of anatase TiO_2 with the symmetries of Eg, B1g, A1g, respectively. And the pure brookite exhibits a characteristic intense band at 153 cm^{-1}, which is covered by the strong band at 142 cm^{-1}. However, the band at 320 cm^{-1}, which can be ascribed to the fundamental vibration modes of brookite TiO_2 with the symmetry of B1g, proves the existence of the brookite in the lattice. These results are consistent with the XRD measurements. Because the percentage of brookite decreases as the increases of the dopant (according to the XRD result, the percentages of brookite in blank-TiO_2, 0.5%V-TiO_2, and 0.32C-0.5%V-TiO_2 are 21.4, 17.8, and 17.7%, respectively), the brookite band at 320 cm^{-1} becomes weaker with the increase in the dopant amount.

No Raman lines due to vanadium oxide can be observed in the vanadium-doped samples, which proves that vanadium is dispersed very well and no vanadium oxide cluster exists. It also confirms that vanadium may be present in the substitutional positions in the lattice of TiO_2.

For the carbon-deposited 0.32C-0.5%V-TiO_2 sample, the Raman peaks between 1000 and 2000 cm^{-1} appear (Figure 7). It is reported that peaks around 1100, 1338, and 1582 cm^{-1} indicate the existence of amorphous carbons with some degrees of graphitic ordering. Therefore the remaining carbon on the

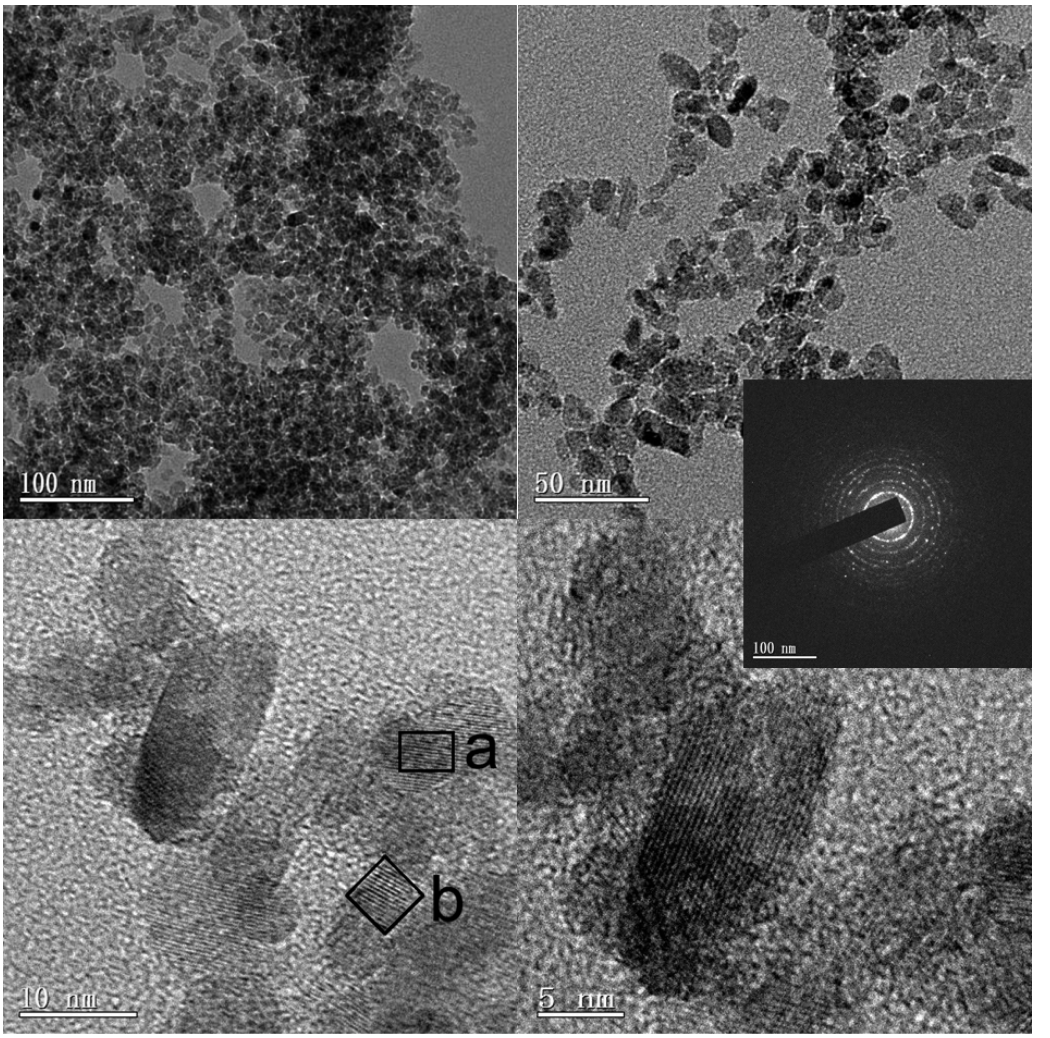

Figure 3. HRTEM images for 0.32C-0.5%V-TiO_2 and its SAED imagine.

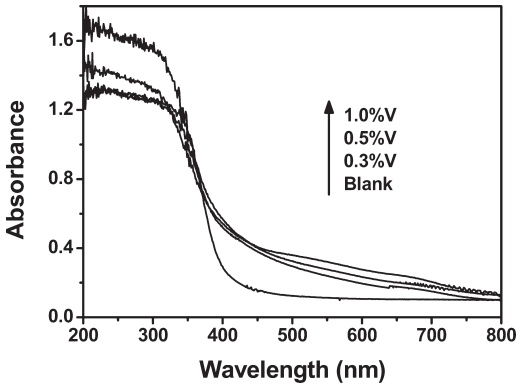

Figure 4. UV−vis diffuse reflectance spectra of blank-TiO_2, 0.3%V-TiO_2, 0.5%V-TiO_2, and 1.0%V-TiO_2.

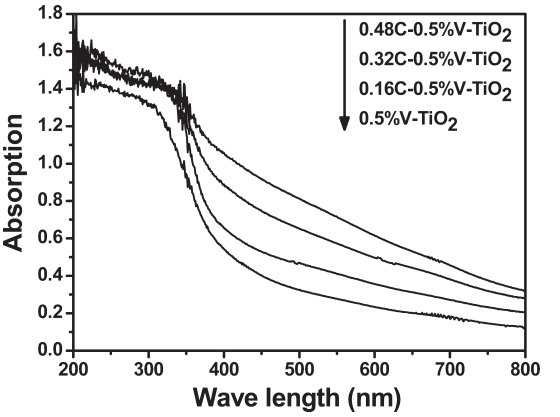

Figure 5. UV−Vis diffuse reflectance spectra of 0.5%V-TiO_2, 0.16C-0.5%V-TiO_2, 0.32C-0.5%V-TiO_2, and 0.48C-0.5%V-TiO_2.

crystalline surface must be present as a stable graphite-like carbonaceous species.[33] It is also noticed that all the peaks observed in Figure 7 shifted to the higher wavelength, which can be attribute to the carbonaceous species formed by the carbon on surface.

3.5. TG Analysis. The TG-DTA profiles of 0.5%V-TiO_2 and 0.32C-0.5%V-TiO_2 are shown in Figure 8. It can be seen that the profiles of the two DTA curves are quite different. Both samples show a single peak at 100 °C, which is due to the loss of physically adsorbed water. 0.32C-0.5%V-TiO_2 shows a single peak at 230 °C, whereas 0.5%V-TiO_2 shows a broad shoulder peak there. These peaks are due to the removal of strongly bound

water or surface hydroxyl. And also some strongly bound water or surface hydroxyl groups on the sample are slowly being eliminated with the rise of temperature from 100 to 400 °C. And both samples also show a single peak at 450 °C, which can be attributed to decomposition of organic compound. 0.32C-0.5%V-TiO_2 shows a unique peak at 550 °C, which is also due to decomposition of organic compound, which comes from the precursor glucose.

Thermogravimetric analysis (TG) is used to estimate the carbon content in the sample. Taking the mass loss of 0.5%V-TiO_2 as a reference, the carbon content can be calculated to be 2.9 wt.% for 0.32C-0.5%V-TiO_2.

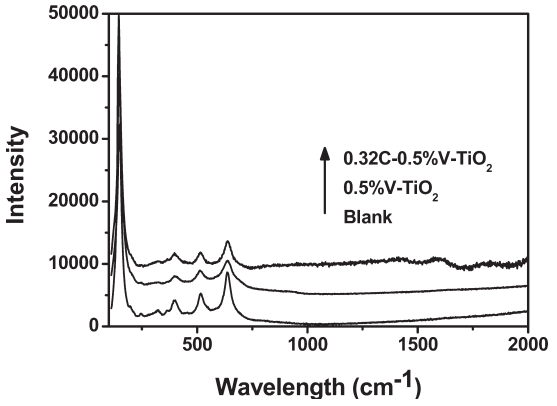

Figure 6. Raman spectra of blank-TiO_2, 0.5%V-TiO_2, and 0.32C-0.5% V-TiO_2.

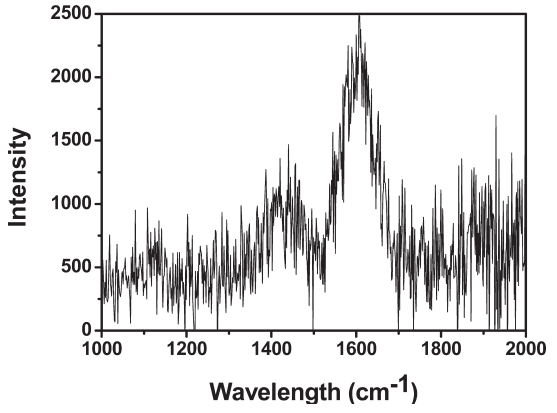

Figure 7. Raman spectrum of 0.32C-0.5%V-TiO_2 in the wavelength region of 1000−2000 cm^{-1}.

3.6. XPS Analysis. Ti 2p XPS spectra of blank-TiO_2 and 0.32C-0.5%V-TiO_2 samples are shown in Figure 9. The binding energies of Ti $2p_{3/2}$ and Ti $2p_{1/2}$ for 0.32C-0.5%V-TiO_2 sample are at 458.4 and 464.0 eV, respectively, which agree with Ti (IV) in titanium oxide. Furthermore, compared with blank-TiO_2, 0.32C-0.5%V-TiO_2 sample exhibits an asymmetrical shoulder at 458.5 eV, which indicates the existence of Ti^{3+}.[21,42] As is well-known, the vanadium has variable valence. So V^{5+} can replace Ti^{4+} site in the lattice, which breaks the charge balance and leads to the produce of Ti^{3+}. It means vanadium doping favors the formation of Ti^{3+} on the surface or subsurface layer of TiO_2.

V $2p^{2/3}$ spectra of 0.5%V-TiO_2 and 0.32C-0.5%V-TiO_2 samples are illustrated in Figure 10. For the 0.5%V-TiO_2 sample, the peak of V $2p^{2/3}$ can be divided into two peaks. The peak at a binding energy of 519.6 eV suggests V^{5+} species, whereas the shoulder at 517.8 eV can be assigned to V^{4+}. V^{4+} and V^{5+} ions were incorporated into the crystal lattice of TiO_2 and no vanadium oxide phase was present; thus, V^{4+} and V^{5+} ions substituted for Ti^{4+} ions and formed a Ti−O−V bond.

The presence of V^{4+} in the mixture catalysts may be due to the reduction of V^{5+} by Ti^{3+} generated during the calcinations of the catalysts. Trifiro[43] suggested a mechanism for the spontaneous reduction of V^{5+} by studying the solid-state preparation of V_2O_5/TiO_2, which showed that dehydroxylation of surface Ti^{4+} sites leads to the formation of Ti^{3+} followed by charge transfer and subsequent reduction of V^{5+} to form stable Ti−O−V bonds during annealing.

The existence of V^{4+} is very critical to the visible light photocatalysis. It can replace the site of Ti^{4+} in the bulk without inducing significant lattice distortion. Furthermore, it can form an impurity energy band V^{4+}/V^{5+} at 2.1 eV, which is lower than conduction band of TiO_2.[27] Therefore, it can alter the electronic properties by trapping a photogenerated hole or injecting an electron to the TiO_2 conduction band to form V^{5+}, which is more stable.

For the 0.32C-0.5%V-TiO_2 sample, the peak of V $2p^{2/3}$ can also be divided into two peaks. However, both of these two peaks shift to higher binding energy. That fact indicates carbon modification increases the density of electron cloud around vanadium ions. Furthermore, the intensity of V^{5+} becomes weaker, whereas the intensity of V^{4+} strengthens. And the calculated ratios of V^{4+} to V^{5+} of 0.5%V-TiO_2 and 0.32C-0.5%V-TiO_2 samples are 0.40 and 1.08, respectively. This means that some V^{5+} ions are reduced to V^{4+} ions by modified carbon. It also indicates that

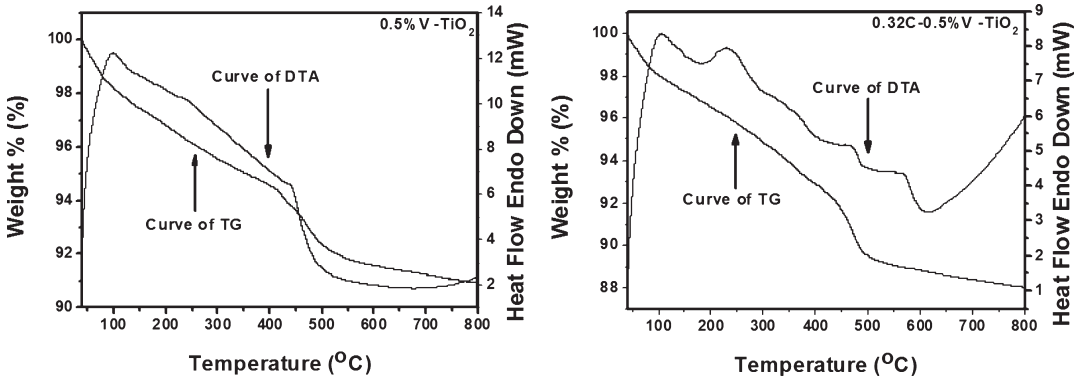

Figure 8. Thermal analysis (TG/DTA) profiles of 0.5%V -TiO_2 (left) and 0.32C-0.5%V -TiO_2 (right).

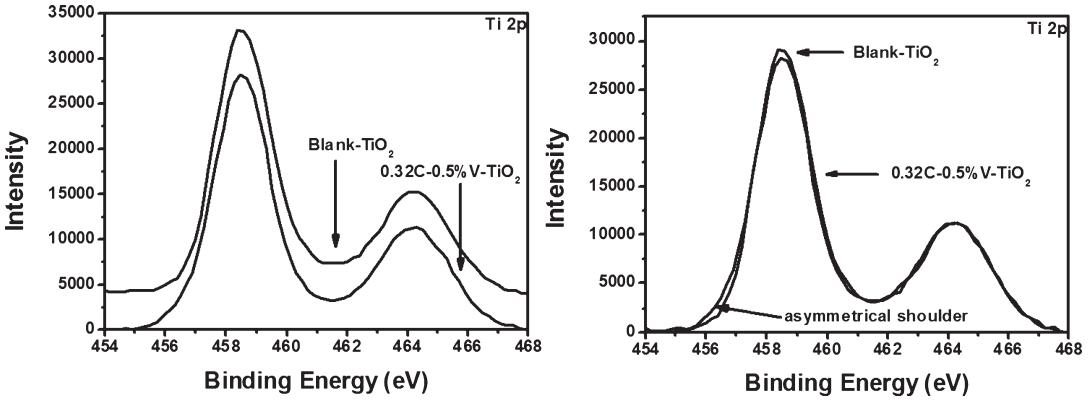

Figure 9. Ti 2p XPS spectra of blank-TiO_2 and 0.32C-0.5%V-TiO_2 samples (left, in the form of waterfall; right, in the normal form).

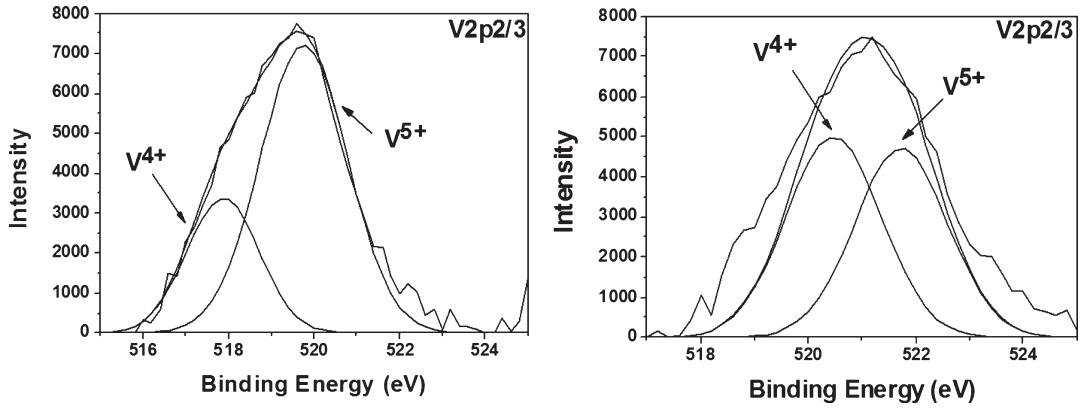

Figure 10. V $2p^{2/3}$ spectra of 0.5%V-TiO_2 (left) and 0.32C-0.5%V-TiO_2 (right).

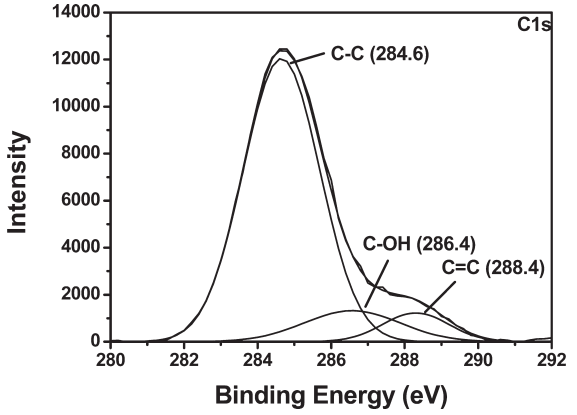

Figure 11. C 1s spectra of 0.32C-0.5%V-TiO_2.

the electron clouds of modified carbon and doped vanadium can be interacted with each other. This could be the foundation of the synergistic effects of vanadium and carbon.

Figure 11 shows the C 1s spectra of 0.32C-0.5%V-TiO_2 sample. The peak of C 1s is divided into three peaks. The peak at 284.6 eV is associated with the adventitious elemental carbon from glucose or internal standard carbon while XPS testing. And the shoulders at 286.6 and 288.4 eV represent the bonds of C−O (C−O−H or C−O−C) and C═O (or O−C−O), respectively, indicating the formation of carbonated species. But there is no significant peak at 281.4 eV resulting from Ti−C bond, which is the evidence of no carbon doping in the lattice.[36] Therefore, it is proved that all the carbon is modified on the surface of the catalysts, and no carbon doping exists.

3.7. Photocatalysis Activity. Figure 12 shows the photocatalytic degradation curves of AO7 over 0.3%V-TiO_2, 0.5%V-TiO_2, and 1.0%V-TiO_2 photocatalysts with different vanadium doping concentration under visible light irradiation in the left graph. It also shows the photocatalytic degradation curves of AO7 over 0.32C-blank-TiO_2, 0.32C-0.3%V-TiO_2, 0.32C-0.5%V-TiO_2, and 0.32C-1.0%V-TiO_2 photocatalysts with the ratio of C:Ti = 0.32 glucose modified with different vanadium doping concentration under visible-light irradiation in the right graph. The photocatalytic reactions of modified samples with different ratio of C:Ti have also been done but not shown here, which give the result that the ratio of C:Ti = 0.32 shows the best photoactivity.

The left graph illustrates that the highest photocatalytic activity is observed at intermediate vanadium concentrations. Thus, in the case of V-doped TiO_2 the dopant amount steadily increases with vanadium contents of 0.3, 0.5, and 1.0%, whereas the reaction rate of degradation exhibits a maximum at 0.5%. As we all know, pure anatase shows no visible light photocatalytic activity and the prepared blank-TiO_2 shows only a litter visible photocatalytic activity (not shown here), so vanadium doping enhances the visible photoactivity of catalysts very well because of formation of an impurity band level.

The right graph shows that all catalysts exhibit better photoactivities after carbon modification. And considering the catalyst

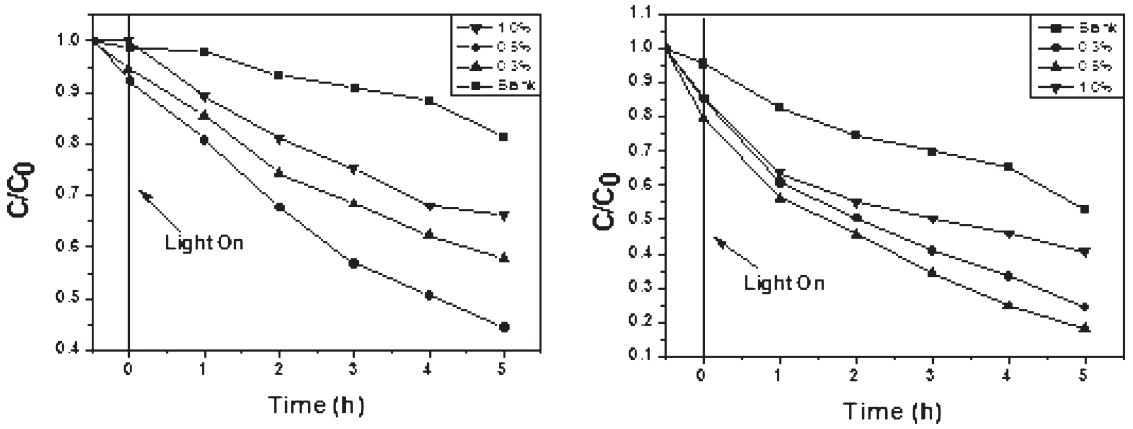

Figure 12. Photocatalytic degradation curves of AO7 on different amounts of vanadium-doped TiO_2 catalysts (left) and 0.32 carbon-modified different amounts of vanadium-doped TiO_2 catalysts (right) under visible-light irradiation (the error limit on data is 1%).

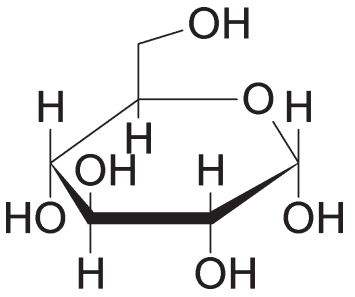

Figure 13. Molecule structure of D-(+)-glucose.

particle size increases slightly, the enhanced activities can be totally attributed to the modified carbon. Furthermore, 0.32C-0.5%V-TiO_2 also exhibits the best activity with that amount of carbon modification.

3.8. Mechanism. The higher photocatalytic activity of carbon-modified vanadium-doped TiO_2 here observed may be attributed to the following reasons: vanadium doping, carbon modification, and synergistic effect between vanadium and carbon.

The vanadium doped into the crystal lattice of TiO_2 modifies the electronic properties of TiO_2. And it influences the photoactivity of catalysts by acting as hole (or electron) trap center within band gap of TiO_2 bulk and alters the e^-/h^+ pair recombination rate through V^{5+}/V^{4+} ions pair. Because the energy level of V^{5+}/V^{4+} lies below the conduction band edge at 2.1 eV,[27] the 3d electron from a V^{4+} center is easily excited into the TiO_2 conduction band under visible-light irradiation and left V^{5+} there, which also helps the visible-light absorption. The photoexcited electron can react with O_2 dissolved in the aqueous solution, generating the superoxide radical anion, which can oxidize and degrade organic compounds. On the other hand, some V^{5+} ions exist on the surface of TiO_2 can bond to oxygen (V=O) there, which can be oxidized to hydroxide radicals by photoexcited holes.[44] The hydroxide radicals can also degrade organic compounds.

Figure 13 illustrates the molecule structure of D-(+)-glucose. It can easily be thermally polyerized to be polyglucose, and furthermore, to be polymerid at higher temperature. The Raman conclusion combined with the results of XPS indicates that all the carbon is modified on the surface and it exists in the form of graphite-like carbonaceous species on the surface of photocatalysts.

Scheme 1. Mechanism for the Synergistic Effects of Vanadium and Carbon

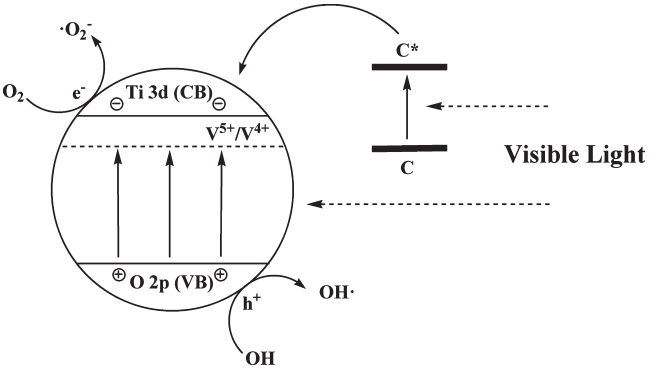

The carbon on the surface could enhance the photoactivity as a photosensitizer, which absorbs visible light and generates an electron into the conduction band, or more easily, into the impurity energy level, V^{5+}/V^{4+}. And the electron there can move to the surface, leading to superoxide radical anion.

The dark absorption results of photocatalysis shown in Figure 12 also prove that carbon modified samples can adsorb more AO7 dye amount than unmodified ones. The BET surface areas of 0.5%V-TiO_2 and 0.32C-0.5%V-TiO_2 samples, which are 117 and 175 m^2/g, respectively, were tested and are shown in Figure S1 in the Supporting Information. The increase of surface area after carbon modification may be due to the accumulation of the carbonated species. And the increased surface area can enhance the adsorption of dyes on the surface of the catalysts through chemical or physical interaction. It is known that the lifetime of the excited electrons are very short and therefore the long distance electrons transfer are kinetically prohibited.[45] Therefore, most photocatalysis happens in the near distance, which means only the dyes absorbed on the surface of catalysts can be photocatalytic degraded. Because carbon modification can increase the dark absorption, it can enhance the photoactivity to some extent in this way.

XPS results indicate that the electron clouds of Ti, V and C can interact. For the carbon modified vanadium doped TiO_2, modified carbon can act as a photosensitizer, absorbing visible light

and impregnating electron to conduction band or impurity energy level. Through trapping photogenerated electrons by V^{5+}/V^{4+} pairs and photogenerated holes by modified carbon, the e^-/h^+ pair are well-separated. Consequently, the quantum efficiency of the photocatalytic reaction of comodified TiO_2 is improved. In other words, the synergistic effects of carbon modification and vanadium doping may not only enhance the utilization efficiency of solar energy due to surface carbon and bulk vanadium narrowing the band gap, but also sufficiently promote the separation of photogenerated holes and electrons and then lead to high photodegradation efficiency of AO7 under the visible-light irradiation (Scheme. 1).

4. CONCLUSIONS

Here, the carbon-modified vanadium-doped titanium dioxide catalysts are synthesized by a low-temperature wet chemical method. The prepared catalysts show small crystallite size, relatively large surface areas, and therefore highly photoactive of degrading AO7 under visible light irradiation. The experimental results show that vanadium is doped into the lattice while carbon is modified on the surface. Both of the carbon species and vanadium ions are beneficial to the utilization of visible light and the separation of photogenerated holes and electrons, which in turn are beneficial to the activity of degrading AO7 under visible-light irradiation. In summary, the synergistic effects between vanadium and carbon lead to enhance the photoactivity of carbon-modified and vanadium-doped TiO_2.

■ ASSOCIATED CONTENT

Supporting Information. Figure of BET results (PDF). This material is available free of charge via the Internet at http://pubs.acs.org.

■ AUTHOR INFORMATION

Corresponding Author
*E-mail: jlzhang@ecust.edu.cn.

■ ACKNOWLEDGMENT

This work has been supported by National Nature Science Foundation of China (20773039, 20977030), National Basic Research Program of China (973 Program, 2007CB613301, 2010CB732306), Science and Technology Commission of Shanghai Municipality (10520709900, 10JC1403900), and the Fundamental Research Funds for the Central Universities.

■ REFERENCES

(1) Fujisima, A.; Honda, K. *Nature* **1972**, *238*, 37.
(2) Hoffmann, M. R.; Martin, S. T.; Choi, W.; Bahnemann, D. W. *Chem. Rev.* **1995**, *95*, 69.
(3) Kaur, A.; Gupta, U. *J. Mater. Chem.* **2009**, *19*, 8279.
(4) Anpo, M.; Takeuchi, M. *J. Catal.* **2003**, *216*, 505.
(5) Sathish, M.; Viswanathan, B.; Viswanath, R. P. *Appl. Catal., B* **2007**, *74*, 307.
(6) Khan, R.; Kim, S. W.; Kim, T.-J.; Nam, C.-M. *Mater. Chem. Phys.* **2008**, *112*, 167.
(7) Colón, G.; Maicu, M.; Hidalgo, M. C.; Navío, J. A. *Appl. Catal., B* **2006**, *67*, 41.
(8) Ji, T.; Liu, Y.; Zhao, H.; Du, H.; Sun, J.; Ge, G. *J. Solid State Chem.* **2010**, *183*, 584.
(9) Hong, X.; Wang, Z.; Cai, W.; Lu, F.; Zhang, J.; Yang, Y.; Ma, N.; Liu, Y. *Chem. Mater.* **2005**, *17*, 1548.
(10) Mu, S.; Long, Y.; Kang, S.-Z.; Mu, J. *Catal. Commun.* **2010**, *11*, 741.
(11) Zhang, M.; Chen, C.; Ma, W.; Zhao, J. *Angew. Chem., Int. Ed.* **2008**, *47*, 9730.
(12) Liu, B.; Wang, X.; Cai, G.; Wen, L.; Song, Y.; Zhao, X. *J. Hazard. Mater.* **2009**, *169*, 1112.
(13) Xing, M.; Zhang, J.; Chen, F. *J. Phys. Chem. C* **2009**, *113*, 12848.
(14) Wu, Y.; Zhang, J.; Xiao, L.; Chen, F. *Appl. Catal., B* **2009**, *88*, 525.
(15) Bak, T.; Nowotny, M. K.; Sheppard, L. R.; Nowotny, J. *J. Phys. Chem. C* **2008**, *112*, 7255.
(16) Shojaie, A. F.; Loghmani, M. H. *Chem. Eng. J.* **2010**, *157*, 263.
(17) Cong, Y.; Zhang, J. L.; Chen, F.; Anpo, M. *J. Phys. Chem. C* **2007**, *111*, 6976.
(18) Cong, Y.; Zhang, J. L.; Chen, F.; Anpo, M.; He, D. N. *J. Phys. Chem. C* **2007**, *111*, 10618.
(19) Wu, Y.; Liu, H.; Zhang, J.; Chen, F. *J. Phys. Chem. C* **2009**, *113*, 14689.
(20) Wu, Y.; Zhang, J.; Xiao, L.; Chen, F. *Appl. Surf. Sci.* **2010**, *256*, 4260.
(21) Xing, M.; Wu, Y.; Zhang, J.; Chen, F. *Nanoscale* **2010**, *2*, 1233.
(22) Xing, M. Y.; Zhang, J. L.; Chen, F. *Appl. Catal., B* **2009**, *89*, 563.
(23) Zhang, J.; Wu, Y.; Xing, M.; Leghari, S. A. K.; Sajjad, S. *Energy Environ. Sci.* **2010**, *3*, 715.
(24) Wu, Z.; Dong, F.; Liu, Y.; Wang, H. *Catal. Commun.* **2009**, *11*, 82.
(25) Yamashita, H.; Harada, M.; Misaka, J.; Takeuchi, M.; Ikeue, K.; Anpo, M. *J. Photochem. Photobiol. A* **2002**, *148*, 257.
(26) Yamashita, H.; Harada, M.; Misaka, J.; Takeuchi, M.; Neppolian, B.; Anpo, M. *Catal. Today* **2003**, *84*, 191.
(27) Yang, X.; Cao, C.; Hohn, K.; Erickson, L.; Maghirang, R.; Hamal, D.; Klabunde, K. *J. Catal.* **2007**, *252*, 296.
(28) Yang, X.; Ma, F. Y.; Li, K. X.; Guo, Y. G.; Hu, J. L.; Li, W.; Huo, M. X.; Guo, Y. H. *J. Hazard. Mater.* **2010**, *175*, 429.
(29) Chen, C.; Long, M.; Zeng, H.; Cai, W.; Zhou, B.; Zhang, J.; Wu, Y.; Ding, D.; Wu, D. *J. Mol. Catal. A: Chem.* **2009**, *314*, 35.
(30) Gao, H.; Ding, C.; Dai, D. *J. Mol. Struct.:THEOCHEM* **2010**, *944*, 156.
(31) Mozia, S.; Toyoda, M.; Inagaki, M.; Tryba, B.; Morawski, A. W. *J. Hazard. Mater.* **2007**, *140*, 369.
(32) Zabek, P.; Eberl, J.; Kisch, H. *Photochem. Photobiol. Sci.* **2009**, *8*, 264.
(33) Zhang, L.-W.; Fu, H.-B.; Zhu, Y.-F. *Adv. Funct. Mater.* **2008**, *18*, 2180.
(34) Chen, F.; Zou, W.; Qu, W.; Zhang, J. *Catal. Commun.* **2009**, *10*, 1510.
(35) Wu, Y.; Xing, M.; Zhang, J.; Chen, F. *Appl. Catal., B* **2010**, *97*, 182.
(36) Zhong, J.; Chen, F.; Zhang, J. *J. Phys. Chem. C* **2009**, *114*, 933.
(37) Zou, W.; Zhang, J.; Chen, F. *Mater. Lett.* **2010**, *64*, 1710.
(38) Zhang, H.; Banfield, J. F. *J. Phys. Chem. B* **2000**, *104*, 3481.
(39) Martinez-Huerta, M. V.; Fierro, J. L. G.; Banares, M. A. *Catal. Commun.* **2009**, *11*, 15.
(40) Gong, X..; Selloni, A. *Phys. Rev. B:Condens. Matter Mater. Phys* **2007**, *76*, 235307.
(41) Penn, R. L.; Banfield, J. F. *Am. Mineral.* **1998**, *83*, 1077.
(42) Adachi, Y.; Kohiki, S.; Wagatsuma, K.; Oku, M. *J. Appl. Phys.* **1998**, *84*, 2123.
(43) Trifirò, F. *Catal. Today* **1998**, *41*, 21.
(44) Klosek, S.; Raftery, D. *J. Phys. Chem. B* **2001**, *105*, 2815.
(45) Tennakone, K.; Bandara, J. *Appl. Catal., A* **2001**, *208*, 335.